CATHERINE E. HOUSECROFT & ALAN G. SHARPE

INORGANIC CHEMISTRY

FIFTH EDITION

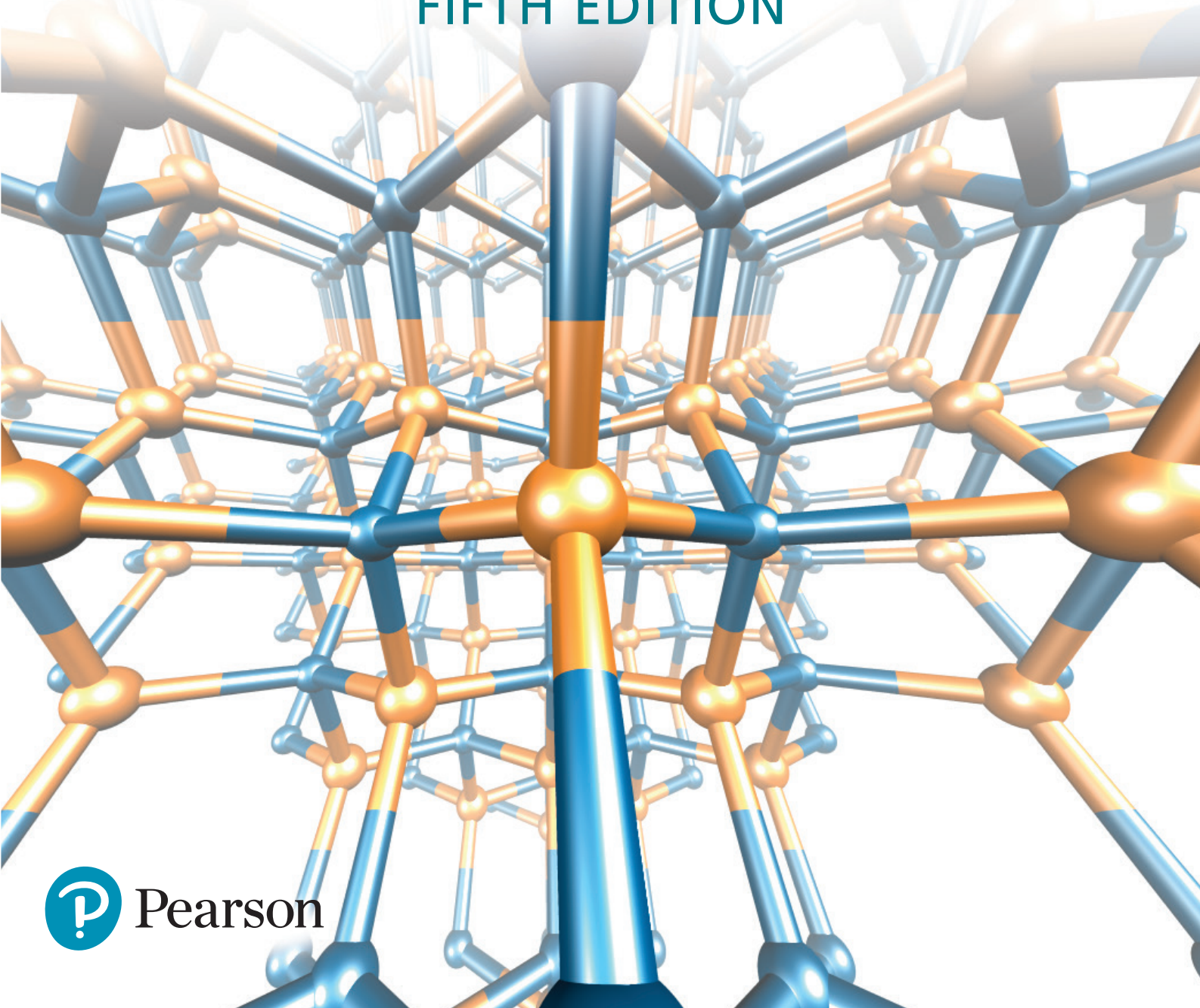

Pearson

Elements

Element	Symbol	Atomic number, Z	Relative atomic mass, A_r[§]/g mol^{-1}	Element	Symbol	Atomic number, Z	Relative atomic mass, A_r[§]/g mol^{-1}	Element	Symbol	Atomic number, Z	Relative atomic mass, A_r[§]/g mol^{-1}
Actinium	Ac	89	[227]	Hafnium	Hf	72	178.49	Praseodymium	Pr	59	140.91
Aluminium	Al	13	26.98	Hassium	Hs	108	[270]	Promethium	Pm	61	[145]
Americium	Am	95	[243]	Helium	He	2	4.00	Protactinium	Pa	91	231.04
Antimony	Sb	51	121.76	Holmium	Ho	67	164.93	Radium	Ra	88	[226]
Argon	Ar	18	39.95	Hydrogen	H	1	1.008	Radon	Rn	86	[222]
Arsenic	As	33	74.92	Indium	In	49	114.82	Rhenium	Re	75	186.21
Astatine	At	85	[210]	Iodine	I	53	126.90	Rhodium	Rh	45	102.91
Barium	Ba	56	137.33	Iridium	Ir	77	192.22	Roentgenium	Rg	111	[281]
Berkelium	Bk	97	[247]	Iron	Fe	26	55.85	Rubidium	Rb	37	85.47
Beryllium	Be	4	9.01	Krypton	Kr	36	83.80	Ruthenium	Ru	44	101.07
Bismuth	Bi	83	208.98	Lanthanum	La	57	138.91	Rutherfordium	Rf	104	[267]
Bohrium	Bh	107	[270]	Lawrencium	Lr	103	[262]	Samarium	Sm	62	150.36
Boron	B	5	10.81	Lead	Pb	82	207.2	Scandium	Sc	21	44.96
Bromine	Br	35	79.91	Lithium	Li	3	6.94	Seaborgium	Sg	106	[269]
Cadmium	Cd	48	112.41	Livermorium	Lv	116	[293]	Selenium	Se	34	78.97
Caesium	Cs	55	132.91	Lutetium	Lu	71	174.97	Silicon	Si	14	28.09
Calcium	Ca	20	40.08	Magnesium	Mg	12	24.31	Silver	Ag	47	107.87
Californium	Cf	98	[251]	Manganese	Mn	25	54.94	Sodium	Na	11	22.99
Carbon	C	6	12.01	Meitnerium	Mt	109	[278]	Strontium	Sr	38	87.62
Cerium	Ce	58	140.12	Mendelevium	Md	101	[258]	Sulfur	S	16	32.06
Chlorine	Cl	17	35.45	Mercury	Hg	80	200.59	Tantalum	Ta	73	180.95
Chromium	Cr	24	52.00	Molybdenum	Mo	42	95.95	Technetium	Tc	43	[97]
Cobalt	Co	27	58.93	Moscovium	Mc	115	[289]	Tellurium	Te	52	127.60
Copernicium	Cn	112	[285]	Neodymium	Nd	60	144.24	Tennessine	Ts	117	[294]
Copper	Cu	29	63.54	Neon	Ne	10	20.18	Terbium	Tb	65	158.93
Curium	Cm	96	[247]	Neptunium	Np	93	[237]	Thallium	Tl	81	204.38
Darmstadtium	Ds	110	[281]	Nickel	Ni	28	58.69	Thorium	Th	90	232.04
Dubnium	Db	105	[270]	Nihonium	Nh	113	[285]	Thulium	Tm	69	168.93
Dysprosium	Dy	66	162.50	Niobium	Nb	41	92.91	Tin	Sn	50	118.71
Einsteinium	Es	99	[252]	Nitrogen	N	7	14.01	Titanium	Ti	22	47.87
Erbium	Er	68	167.26	Nobelium	No	102	[259]	Tungsten	W	74	183.84
Europium	Eu	63	151.96	Oganesson	Og	118	[294]	Uranium	U	92	283.03
Fermium	Fm	100	[257]	Osmium	Os	76	190.23	Vanadium	V	23	50.94
Flerovium	Fl	114	[289]	Oxygen	O	8	16.00	Xenon	Xe	54	131.29
Fluorine	F	9	19.00	Palladium	Pd	46	106.42	Ytterbium	Yb	70	173.04
Francium	Fr	87	[223]	Phosphorus	P	15	30.97	Yttrium	Y	39	88.91
Gadolinium	Gd	64	157.25	Platinum	Pt	78	195.08	Zinc	Zn	30	65.38
Gallium	Ga	31	69.72	Plutonium	Pu	94	[244]	Zirconium	Zr	40	91.22
Germanium	Ge	32	72.63	Polonium	Po	84	[209]				
Gold	Au	79	196.97	Potassium	K	19	39.10				

[§]Where an element does not possess a stable isotope, a mass number in [ ] is given; the mass number given is for the longest-lived isotope of the element. For each of Th, Pa and U, the value of A_r is based on the terrestrial isotopic composition.

Table 11.1 Some physical properties of the alkali metals, M, and their ions, M^+.

Property	Li	Na	K	Rb	Cs
Atomic number, Z	3	11	19	37	55
Ground state electronic configuration	[He]$2s^1$	[Ne]$3s^1$	[Ar]$4s^1$	[Kr]$5s^1$	[Xe]$6s^1$
Enthalpy of atomization, $\Delta_a H^\circ(298\,K)$ / kJ mol^{-1}	161	108	90	82	78
Dissociation enthalpy of M–M bond in M_2 (298 K) / kJ mol^{-1}	110	74	55	49	44
Melting point, mp / K	453.5	371	336	312	301.5
Boiling point, bp / K	1615	1156	1032	959	942
Standard enthalpy of fusion, $\Delta_{fus}H^\circ$(mp) / kJ mol^{-1}	3.0	2.6	2.3	2.2	2.1
First ionization energy, IE_1 / kJ mol^{-1}	520.2	495.8	418.8	403.0	375.7
Second ionization energy, IE_2 / kJ mol^{-1}	7298	4562	3052	2633	2234
Metallic radius, r_{metal} / pm†	152	186	227	248	265
Ionic radius, r_{ion} / pm‡	76	102	138	149	170
Standard enthalpy of hydration of M^+, $\Delta_{hyd}H^\circ(298\,K)$ / kJ mol^{-1}	−519	−404	−321	−296	−271
Standard entropy of hydration of M^+, $\Delta_{hyd}S^\circ(298\,K)$ / J K^{-1} mol^{-1}	−140	−110	−70	−70	−60
Standard Gibbs energy of hydration of M^+, $\Delta_{hyd}G^\circ(298\,K)$ / kJ mol^{-1}	−477	−371	−300	−275	−253
Standard reduction potential, $E^\circ_{M^+/M}$ / V	−3.04	−2.71	−2.93	−2.98	−3.03
NMR active nuclei (% abundance, nuclear spin)	^{6}Li (7.5, $I = 1$); ^{7}Li (92.5, $I = \frac{3}{2}$)	^{23}Na (100, $I = \frac{3}{2}$)	^{39}K (93.3, $I = \frac{3}{2}$); ^{41}K (6.7, $I = \frac{3}{2}$)	^{85}Rb (72.2, $I = \frac{5}{2}$); ^{87}Rb (27.8, $I = \frac{3}{2}$)	^{133}Cs (100, $I = \frac{7}{2}$)

† For 8-coordinate atom in body-centred cubic metal; compare values for 12-coordinate atoms in Appendix 6.
‡ For 6-coordination.

the non-luminous Bunsen flame, a characteristic flame colour is observed (Li, crimson; Na, yellow; K, lilac; Rb, red-violet; Cs, blue) and this *flame* test is used in *qualitative* analysis to identify the M^+ ion. In *quantitative* analysis, use is made of the characteristic atomic spectrum in *atomic absorption spectroscopy* (see Section 4.3).

Worked example 11.1 The Na_2 molecule

Construct an MO diagram for the formation of Na_2 from two Na atoms using only the valence orbitals and electrons of Na. Use the MO diagram to determine the bond order in Na_2.

The atomic number of Na is 11.

The ground state electronic configuration of Na is $1s^2 2s^2 2p^6 3s^1$ or [Ne]$3s^1$.

The valence orbital of Na is the 3*s*.

An MO diagram for the formation of Na_2 is:

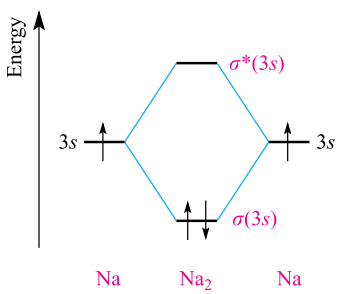

Bond order = $\frac{1}{2}$[(number of bonding electrons) – (number of antibonding electrons)]

Bond order in $Na_2 = \frac{1}{2} \times 2 = 1$

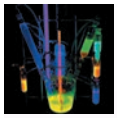

APPLICATIONS

Box 11.2 Keeping time with caesium

In 1993, the National Institute of Standards and Technology (NIST) brought into use a caesium-based atomic clock called NIST-7 which kept international standard time to within one second in 10^6 years. The system depends upon repeated transitions from the ground to a specific excited state of atomic Cs, and the monitoring of the frequency of the electromagnetic radiation emitted.

In 1995, the first caesium fountain atomic clock was constructed at the Paris Observatory in France. A fountain clock, NIST-F1, was introduced in 1999 in the US to function as the country's primary time and frequency standard. In 2014, NIST-F1 was superseded by NIST-F2 which is accurate to within one second in 300×10^6 years, approximately three times more accurate than NIST-F1. In the UK, the National Physics Laboratory's caesium fountain atomic clock NPL-CsF2 (shown in the photograph) is accurate to within one second in 138×10^6 years. While earlier caesium clocks observed Cs atoms at ambient temperatures, caesium fountain clocks use lasers to slow down and cool the atoms to temperatures approaching 0 K. Current atomic clock research is focusing on instruments based on optical transitions of neutral atoms or of a single ion (e.g. $^{88}Sr^+$). Progress in this area became viable after 1999 when optical counters based on femtosecond lasers (see Box 26.2) became available.

Extremely accurate time-keeping is fundamental to many technological advances such as global positional system (GPS) satellite receivers. Mobile phones and laptops with built-in clocks (which we assume are accurate!) are part of our everyday lives.

The caesium fountain atomic clock NPL-CsF2 in the National Physics Laboratory in the UK.

Further reading

M. Chalmers (2009) *New Scientist*, vol. 201, issue 2694, p. 39 – 'Every second counts'.
T.P. Heavner *et al.* (2014) *Metrologia*, vol. 51, p. 174 – 'First accuracy evaluation of NIST-F2'.
R. Le Targat *et al.* (2013) *Nature Commun.*, vol. 4, p. 2109 – 'Experimental realization of an optical second with strontium lattice clocks'.
R. Li, K. Gibble and K. Szymaniec (2011) *Metrologia*, vol. 48, p. 283 – 'Improved accuracy of the NPL-CsF2 primary frequency standard: evaluation of distributed cavity phase and microwave lensing frequency shifts'.
Y. Ovchinnikov and G. Marra (2011) *Metrologia*, vol. 48, p. 87 – 'Accurate rubidium atomic fountain frequency standard'.
M. Takamoto, F.-L. Hong, R. Higashi and H. Katori (2005) *Nature*, vol. 435, p. 321 – 'An optical lattice clock'.
R. Wynands and S. Weyers (2005) *Metrologia*, vol. 42, p. S64 – 'Atomic fountain clocks'.
www.nist.gov/pml/time-and-frequency-division/primary-standard-nist-f1/

Self-study exercises

1. Why is it not necessary to include the 1*s*, 2*s* and 2*p* orbitals and electrons in the MO description of the bonding in Na_2?
2. Use the MO diagram for Na_2 to determine whether Na_2 is paramagnetic or diamagnetic. [*Ans*: Diamagnetic]

See end-of-chapter problem 11.5 for an extension of these exercises.

Radioactive isotopes

In addition to the radioactivity of Fr, 0.02% of naturally occurring K consists of ^{40}K which decays according to scheme 11.2.

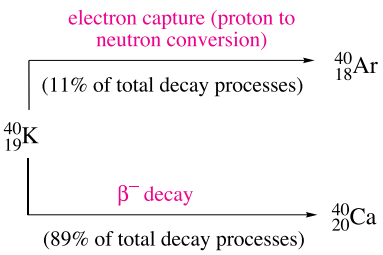

(11.2)

The overall half-life for both the β-decay and electron capture is 1.25×10^9 yr.

The decay of ^{40}K provides the human body with a natural source of radioactivity, albeit at very low levels. The decay from ^{40}K to ^{40}Ar is the basis of a technique for dating minerals (e.g. biotite, hornblende and volcanic rocks). When volcanic magma cools, ^{40}Ar formed from the decay of ^{40}K remains trapped in the mineral. Crushing and heating rock samples releases argon, and the amount of ^{40}Ar present

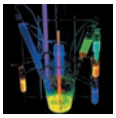

APPLICATIONS

Box 11.3 Alkali metal ion batteries

The sodium/sulfur battery operates around 570–620 K and consists of a molten sodium anode and a liquid sulfur cathode which contains a carbon fibre matrix for conduction. The anode and cathode are separated by a solid β-alumina electrolyte (see Section 28.2). The cell reaction is:

$$2Na(l) + nS(l) \longrightarrow Na_2S_n(l) \qquad E_{cell} = 2.08\,V$$

and this is reversed when the battery is recharged by changing the polarity of the cell. In the 1990s, it appeared that sodium/sulfur batteries may have potential application in the electric vehicle (EV) market, but the high operating temperature of the sodium/sulfur battery is a drawback to the motor industry, and other battery technologies have superseded these batteries for electric and hybrid electric vehicles. Stationary sodium/sulfur batteries are used for energy storage, notably in Japan. This application follows from the fact that self-discharge from sodium/sulfur batteries occurs only at very low levels.

An important advance in battery technology has been the development of rechargeable, high energy-density lithium-ion (Li-ion) batteries, first introduced to the commercial market in 1991. Since then, the market has grown enormously; in 2015, 35% of Li metal produced globally ended up in rechargeable Li-ion batteries. The Li-ion battery has a cell potential of 3.6 V and consists of a positive $LiCoO_2$ electrode separated from a graphite electrode by a solid electrolyte across which Li^+ ions can migrate when the cell is charging. In commercial Li-ion batteries, the electrolyte is usually $LiPF_6$ in a solution of two or more alkylcarbonates. Li-ion batteries are manufactured in a discharged state. Solid $LiCoO_2$ adopts an α-$NaFeO_2$ structure type in which the O atoms are approximately cubic close-packed. The octahedral holes are occupied by M(I) or M'(III) (Li^+ or Co^{3+} in $LiCoO_2$) in such a way that the different metal ions are arranged in layers. During charging, Li^+ ions move out of these layers, are transported across the electrolyte, and are intercalated by the graphite (see Section 14.4). During discharge of the cell, the Li^+ ions return to the metal oxide lattice. The cell reaction can be represented as follows:

$$LiCoO_2 + C_6(\text{graphite}) \underset{\text{discharge}}{\overset{\text{charge}}{\rightleftharpoons}} Li_{1-x}CoO_2 + Li_xC_6(\text{intercalated graphite})$$

The cobalt centres are redox active, some being oxidized from Co(III) to Co(IV) as Li^+ is removed from $LiCoO_2$. The crucial factor in lithium-ion batteries is that both electrodes are able to act as hosts for Li^+ ions. Rechargeable, Li-ion batteries now dominate the market for small electronic devices such as laptop computers, iPads, mobile phones, iPods and MP3 players, and in electric bicycles and cordless power tools.

A disadvantage of Li-ion batteries containing cobalt is their relatively high cost. Current research strategies are aimed at finding replacement electrode materials both to increase battery performance and to reduce cost. Two contenders are $LiMn_2O_4$ and $LiFePO_4$. $LiMn_2O_4$ has a spinel structure (see Box 13.7) and when coupled with a graphite electrode forms a Li-ion battery, the cell reaction of which is summarized below:

$$LiMn_2O_4 + C_6(\text{graphite}) \underset{\text{discharge}}{\overset{\text{charge}}{\rightleftharpoons}} Li_{1-x}Mn_2O_4 + Li_xC_6(\text{intercalated graphite})$$

Applications of this type of Li-ion battery include those in hybrid electric vehicles (HEVs). Manufacturers including

A lithium-ion battery pack for General Motors' electric vehicle, the Chevrolet Volt, which has been on the market since 2011.

Toyota and Honda produce hybrid electric and plug-in electric vehicles (rechargeable from an external power supply when the car is parked) incorporating Li-ion batteries, but the first mass-produced HEV containing a Li-ion battery was launched by Mercedes-Benz in 2009. In the S400 Blue Hybrid, a 120 V Li-ion battery pack powers an electric motor which works in conjunction with an internal combustion engine, the operating mode being computer controlled. A regenerative braking system (see Box 10.5) converts kinetic energy to electrical energy which is stored in the battery, and the electrical motor also recovers energy during deceleration.

Graphite anodes currently employed in commercial Li-ion batteries have a low theoretical charge capacity (372 mAh g^{-1}). This must be improved for commercial use of Li-ion batteries in electric vehicles and other high-energy storage applications. Cutting-edge research is being carried out into the replacement of the intercalation reactions discussed above by alloying reactions. For example, Li reacts with Si to give alloys such as $Li_{15}Si_4$ and $Li_{22}Si_5$, and the theoretical charge capacity of Si is 3579 mAh g^{-1}. Despite this high capacity, bulk Si suffers from a large variation in volume during battery charging and discharging. A viable compromise is the use of C/Si composites, for example, the addition of Si to graphite produces anodes with greatly improved capacity.

Further reading on lithium-ion batteries

L. Liu, J. Lyu, T. Li and T. Zhao (2016) *Nanoscale*, vol. 8, p. 701 – 'Well-constructed silicon-based materials as high-performance lithium-ion battery anodes'.

D. Ma, Z. Cao and A. Hu (2014) *Nano-Micro Lett.*, vol. 6, p. 347 – 'Si-Based anode materials for Li-ion batteries: A mini review'.

N. Nitta and G. Yushin (2014) *Part. Part. Syst. Charact.*, vol. 31, p. 317 – 'High-capacity anode materials for lithium-ion batteries: Choice of elements and structures for active particles'.

C.-M. Park, J.-H. Kim, H. Kim and H.-J. Sohn (2010) *Chem. Soc. Rev.*, vol. 39, p. 3115.

B. Scrosati and J. Garche (2010) *J. Power Sources*, vol. 195, p. 2419.

F.T. Wagner, B. Lakshmanan and M.F. Mathias (2010) *J. Phys. Chem. Lett.*, vol. 1, p. 2204.

can be determined by mass spectrometry. Atomic absorption spectroscopy is used to determine the ^{40}K content. The age of the mineral can be estimated from the ratio of $^{40}K : {}^{40}Ar$.[†]

NMR active nuclei

Each of the alkali metals has at least one NMR active nucleus (Table 11.1), although not all nuclei are of sufficient sensitivity to permit their routine use. For examples of NMR spectroscopy utilizing *s*-block metals, see Section 4.8 and worked example 23.1.

11.4 The metals

Appearance

The metals Li, Na, K and Rb are silvery-white, but Cs has a golden-yellow cast. All are soft, Li the least so, and the trend is consistent with their melting points (Table 11.1). The particularly low melting point of Cs (301.5 K) means that it may be a liquid at ambient temperatures in hot climates.

Reactivity

We have already described the behaviour of the metals in liquid NH_3 (see Section 9.6). The ultimate products are alkali metal amides, MNH_2 (see eq. 9.28), and $LiNH_2$, $NaNH_2$ and KNH_2 are important reagents in organic synthesis. In the solid state, these amides adopt structures consisting of cubic close-packed $[NH_2]^-$ ions with M^+ ions occupying half the tetrahedral holes.

Worked example 11.2 Structure of $NaNH_2$

The solid state structure of $NaNH_2$ can be approximately described as consisting of an fcc arrangement of amide ions with Na^+ ions occupying half the tetrahedral holes. To which structure type (or prototype structure) does this correspond?

A face-centred cubic (i.e. cubic close-packed) arrangement of $[NH_2]^-$ ions (assuming each is spherical) corresponds to the following unit cell:

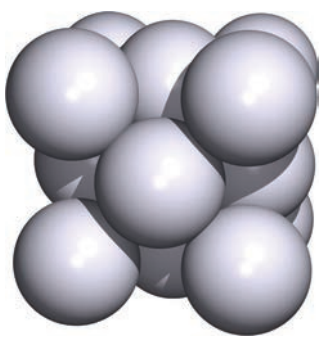

There are eight tetrahedral holes within the unit cell. The Na^+ ions occupy half of these interstitial sites:

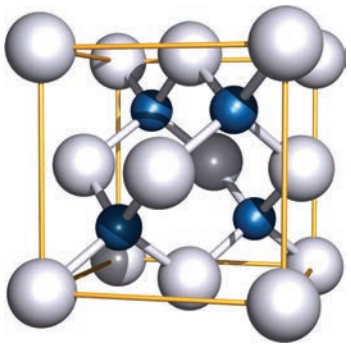

$NaNH_2$ adopts a zinc blende (ZnS) structure (compare with Fig. 6.21b).

Self-study exercises

1. Use the diagram of the unit cell for sodium amide to confirm the $1:1$ $Na^+ : [NH_2]^-$ ratio.
2. Using the diagram of the unit cell of $NaNH_2$, determine the coordination number of each $[NH_2]^-$ ion. To check your answer, think how this coordination number must be related to that of an Na^+ ion.

Although Li, Na and K are stored under a hydrocarbon solvent to prevent reaction with atmospheric O_2 and water vapour, they can be handled in air, provided undue exposure is avoided; Rb and Cs should be handled in an inert atmosphere. Lithium reacts quickly with water (eq. 11.3); Na reacts vigorously, and K, Rb and Cs react violently with the ignition of H_2 produced.

$$2Li + 2H_2O \longrightarrow 2LiOH + H_2 \qquad (11.3)$$

Sodium is commonly used as a drying agent for hydrocarbon and ether solvents. Sodium should *never* be used to dry halogenated solvents (see eq. 14.47). The disposal of excess Na must be carried out with care and usually involves the reaction of Na with propan-2-ol:

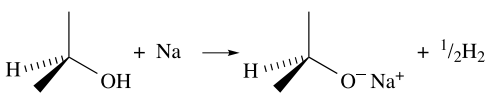

This is a less vigorous, and therefore safer, reaction than that of Na with H_2O or a low molecular mass alcohol. An alternative method for disposing of small amounts of Na involves adding H_2O to a sand-filled ceramic container (e.g. plant pot) in which the metal has been buried. The

[†] For a discussion of ^{40}K–^{40}Ar dating, see: W.A. Howard (2005) *J. Chem. Educ.*, vol. 82, p. 1094.

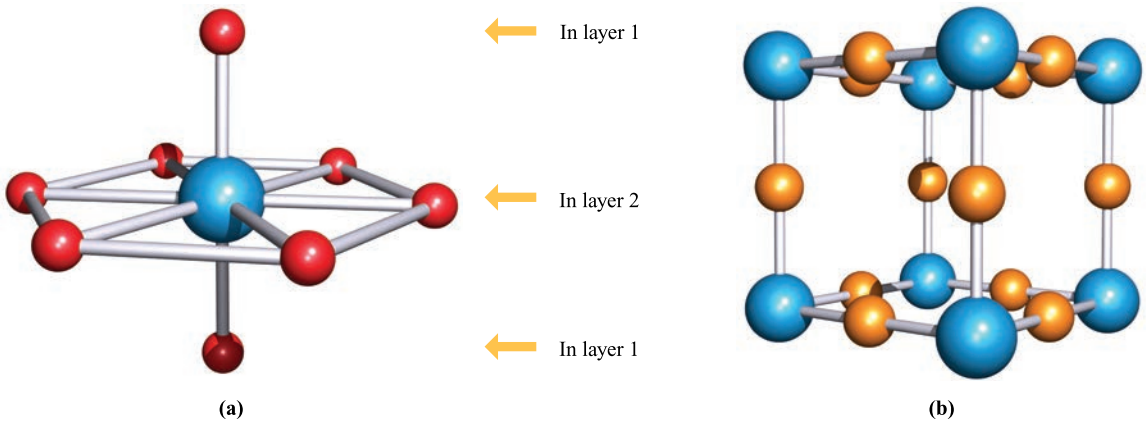

Fig. 11.4. (a) The solid state structure of Li_3N consists of layers of N^{3-} and Li^+ ions (ratio 1 : 2) alternating with layers of Li^+ ions; the latter are arranged such that they lie over the N^{3-} ions. Each N centre is in a hexagonal bipyramidal (8-coordinate) environment; there are two types of Li^+ ion, those in layer 1 are 2-coordinate, and those in layer 2 are 3-coordinate with respect to the N centres (see end-of-chapter problem 11.12). (b) The unit cell of sodium nitride; Na_3N adopts an anti-ReO_3 structure. Colour code: N, blue; Li, red; Na, orange.

conversion of Na to NaOH occurs slowly, and the NaOH reacts with the sand (i.e. SiO_2) to yield sodium silicate.[†]

All the group 1 metals react with the halogens (eq. 11.4) and H_2 when heated (eq. 11.5). The energetics of metal hydride formation are essentially like those of metal halide formation, being expressed in terms of a Born–Haber cycle (see Section 6.14).

$$2M + X_2 \longrightarrow 2MX \qquad X = \text{halogen} \qquad (11.4)$$

$$2M + H_2 \longrightarrow 2MH \qquad (11.5)$$

Self-study exercises

1. Calculate $\Delta_{\text{lattice}}H^{\circ}(\text{NaH, s})$ using a Born–Haber cycle; $\Delta_f H^{\circ}(\text{NaH, s}) = -56.3\,\text{kJ mol}^{-1}$, and see the Appendices for other data.

[*Ans.* $-805.1\,\text{kJ mol}^{-1}$]

2. Use the VBT approach (Section 6.16) to estimate a value for the lattice energy of NaH.

[*Ans.* $-807\,\text{kJ mol}^{-1}$]

Lithium reacts spontaneously with N_2, and reaction 11.6 occurs at 298 K to give red-brown, moisture-sensitive lithium nitride. Solid Li_3N has an interesting structure (Fig. 11.4a) and a high ionic conductivity (see Section 28.2). Attempts to prepare the binary nitrides of the later alkali metals were not successful until 2002. Na_3N (which is very moisture-sensitive) may be synthesized in a vacuum chamber by depositing atomic sodium and nitrogen onto a cooled sapphire substrate and then heating to room temperature. The structure of Na_3N is very different from that of Li_3N (Fig. 11.4), with Na_3N adopting an anti-ReO_3 structure (see Fig. 22.4 for ReO_3) in which the Na^+ ions are 2-coordinate and the N^{3-} ions are octahedrally sited.

$$6Li + N_2 \longrightarrow 2Li_3N \qquad (11.6)$$

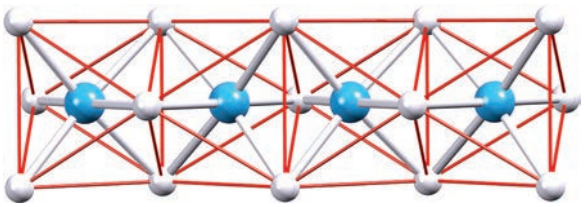

Fig. 11.5. Part of one column of face-sharing octahedra (shown in red) of K^+ ions in the hexagonal phase of K_3N. This is an anti-TiI_3 structure-type. Colour code: K, pale grey; N, blue.

An analogous synthetic method to that used to prepare Na_3N was reported in 2004 for the synthesis of K_3N from potassium and nitrogen.[‡] Two phases of K_3N have been identified. The hexagonal phase adopts an anti-TiI_3 structure; the K^+ ions lie at the vertices of face-sharing octahedra (Fig. 11.5), forming columns which lie parallel to one another in the lattice. The coordination numbers of the K^+ and N^{3-} ions are 2 and 6, respectively. Reactions of the alkali metals with O_2 are discussed in Section 11.6.

Acetylides, M_2C_2, are formed when Li or Na is heated with carbon. These compounds can also be prepared by treating the metal with C_2H_2 in liquid NH_3. Reactions

[†] See: H.W. Roesky (2001) *Inorg. Chem.*, vol. 40, p. 6855 – 'A facile and environmentally friendly disposal of sodium and potassium with water'.

[‡] D. Fischer, Z. Cancarevic, J.C. Schön and M. Jansen (2004) *Z. Anorg. Allg. Chem.*, vol. 630, p. 156.

between K, Rb or Cs and graphite lead to a series of *intercalation compounds* MC_n (n = 8, 24, 36, 48 and 60) in which the alkali metal atoms are inserted between the layers in a graphite host lattice (see structure 14.2 and Fig. 14.4a). For a given formula, the compounds are structurally similar and exhibit similar properties, irrespective of the metal. Under high-pressure conditions, $MC_{4–6}$ (M = K, Rb, Cs) can be formed. In contrast, the intercalation of lithium into graphite gives LiC_6, LiC_{12}, LiC_{18} and LiC_{27}. At high pressures, $LiC_{2–4}$ can be produced. In contrast to the other alkali metals, sodium does not intercalate into graphite. However, in 2014, it was discovered that solvated Na^+ ion intercalation can occur. This may lead towards applications of Na/solvent co-intercalation anode materials for rechargeable batteries.[†] We return to graphite intercalation compounds in Section 14.4. Note that, in contrast to the above intercalations, intercalation in Li-ion batteries (Box 11.3) does not involve Li/Li^+ redox chemistry.

The alkali metals dissolve in Hg to give amalgams (see Box 22.2). Sodium amalgam is a liquid only when the percentage of Na is low. It is a useful reducing agent in inorganic and organic chemistry, and can be used in aqueous media because there is a large overpotential for the discharge of H_2.

An innovative method of handling alkali metals is to absorb them into silica gel, thus providing a convenient source of the metals as powerful reducing agents, e.g. in Birch reductions:

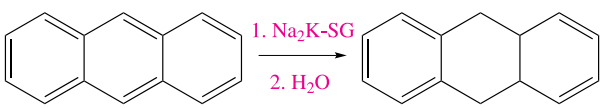

97% yield

Na_2K-SG = Na_2K alloy in silica gel

Foreseeable applications of these materials are in the use of continuous-flow columns for reduction reactions in, for example, the pharmaceutical industry. The silica gel–alkali metal powders react quantitatively with water, liberating H_2. Since the powders are easily handled and stored, they have the potential to act as a 'supply-on-demand' source of H_2,[‡] and are now available commercially.

11.5 Halides

The MX halides (see Chapter 6 for structures) are prepared by direct combination of the elements (eq. 11.4) and all the halides have large negative $\Delta_f H^o$ values. However, Table 11.2 shows that for X = F, values of $\Delta_f H^o(MX)$ become *less negative* down the group, while the reverse trend is true for X = Cl, Br and I. For a given metal, $\Delta_f H^o(MX)$ always becomes less negative on going from MF to MI. These generalizations can be explained in terms of a Born–Haber cycle. Consider the formation of MX (eq. 11.7) and refer to Fig. 6.27.

$$\Delta_f H^o(MX, s) = \underbrace{\{\Delta_a H^o(M, s) + IE_1(M, g)\}}_{\text{metal-dependent term}} + \underbrace{\{\Delta_a H^o(X, g) + \Delta_{EA} H(X, g)\}}_{\text{halide-dependent term}} + \Delta_{lattice} H^o(MX, s) \quad (11.7)$$

For MF, the variable quantities are $\Delta_a H^o(M)$, $IE_1(M)$ and $\Delta_{lattice} H^o(MF)$, and similarly for each of MCl, MBr and MI. The sum of $\Delta_a H^o(M)$ and $IE_1(M)$ gives for the formation of Li^+ 681, of Na^+ 604, of K^+ 509, of Rb^+ 485 and of Cs^+ 454 kJ mol^{-1}. For the fluorides, the trend in the values of $\Delta_f H^o(MF)$ depends on the relative values of $\{\Delta_a H^o(M) + IE_1(M)\}$ and $\Delta_{lattice} H^o(MF)$ (Table 11.2), and similarly for chlorides, bromides and iodides. Inspection of the data shows that the variation in $\{\Delta_a H^o(M) + IE_1(M)\}$ is *less* than the variation in $\Delta_{lattice} H^o(MF)$, but *greater* than the variation in $\Delta_{lattice} H^o(MX)$ for X = Cl, Br and I. This is because lattice energy is proportional to $1/(r_+ + r_-)$ (see Section 6.13) and so variation in $\Delta_{lattice} H^o(MX)$ for a given halide is greatest when r_- is smallest (for F^-) and least when r_- is largest (for I^-). Considering the halides of a given metal (eq. 11.7), the small change in the term $\{\Delta_a H^o(X) + \Delta_{EA} H(X)\}$ (−249, −228, −213, −188 kJ mol^{-1} for F, Cl, Br, I respectively) is outweighed by the decrease in $\Delta_{lattice} H^o(MX)$. In Table 11.2, note that the *difference* between the values of $\Delta_f H^o(MF)$ and $\Delta_f H^o(MI)$ *decreases* significantly as the size of the M^+ ion *increases*.

The solubilities of the alkali metal halides in water are determined by a delicate balance between lattice energies and Gibbs energies of hydration (see Section 7.9 for $\Delta_{sol} G^o$ and $\Delta_{hyd} G^o$). LiF has the highest lattice energy of the group 1 metal halides and is only sparingly soluble, but solubility relationships among the other halides call for detailed discussion beyond the scope of this book.[*] The salts LiCl, LiBr, LiI and NaI are soluble in some *O*-donor organic solvents, e.g. LiCl dissolves in THF and MeOH. Complexation of the Li^+ or Na^+ ion by the *O*-donors is likely in all cases (see Section 11.8). Both LiI and NaI are very soluble in liquid NH_3, forming complexes; the unstable complex $[Na(NH_3)_4]I$ has been isolated and contains a tetrahedrally coordinated Na^+ ion.

In the vapour state, alkali metal halides are present mainly as ion-pairs, but measurements of M−X bond distances and

[†] See: H. Kim *et al.* (2015) *Energy Environ. Sci.*, vol. 8, p. 2963 – 'Sodium intercalation chemistry in graphite'.

[‡] See: J.L. Dye *et al.* (2005) *J. Am. Chem. Soc.*, vol. 127, p. 9338; M. Shatnawi *et al.* (2007) *J. Am. Chem. Soc.*, vol. 129, p. 1386.

[*] For further discussion, see: W.E. Dasent (1984) *Inorganic Energetics*, 2nd edn, Cambridge University Press, Cambridge, Chapter 5.